Astronomy & Astrophysics manuscript no. ms˙v28
December 13, 2013

The Effects of Orbital Environment on X-ray CCD Performance

Catherine E. Grant, Beverly LaMarr, Eric D. Miller, and Marshall W. Bautz

Kavli Institute for Astrophysics and Space Research, Massachusetts Institute of Technology, Cambridge, MA 02139, USA e-mail: `cgrant@space.mit.edu`

ABSTRACT

Context. **Ignore the abstract - isn't updated yet.** The performance of CCD detectors aboard orbiting X-ray observatories slowly degrades due to accumulating radiation damage.
Aims. In an effort to understand the relationship between CCD spectral resolution, radiation damage, and the on-orbit particle background, we attempt to identify differences arising in the performance of two CCD-based instruments: the Advanced CCD Imaging Spectrometer (ACIS) aboard the *Chandra X-ray Observatory*, and the X-ray Imaging Spectrometer (XIS) aboard the *Suzaku X-ray Observatory*.
Methods. We compare the performance evolution of front- and back-illuminated CCDs with one another and with that of very similar detectors installed in the ACIS instrument aboard *Chandra*, which is in a much higher orbit than *Suzaku*. We identify effects of the differing radiation environments as well as those arising from structural differences between the two types of detector.
Results. There are some differences and these are they. **Abstract needs help - don't forget to come back to this!!**

Key words. some keywords

1. Introduction

Charged-coupled devices (CCDs) as astronomical X-ray detectors have become nearly ubiquitous since their their first use in sounding rocket flights in the late 1980s. CCDs provide excellent quantum efficiency with moderate spectral resolution over a broad energy range (~0.1–10 keV) and are well-suited as imaging spectrometers as well as readout detectors for dispersive gratings. Currently, CCDs are focal plane detectors in five operating X-ray observatories from NASA, ESA and JAXA, and are planned to be part of many upcoming missions.

Radiation damage is a common concern in all spacecraft components. One symptom of radiation damage in CCDs is an increase in the number of charge traps (**?**) **Ref TBA**. When charge is transferred across the CCD to the readout, some portion can be captured by the traps and gradually re-emitted. If the original charge packet has been transferred away before the traps re-emit, the captured charge is "lost" to the charge packet. This process is quantified as charge transfer inefficiency (CTI), the fractional charge loss per pixel. As a result, the amount of charge (or the pulseheight) read out from the instrument decreases with increasing transfer distance; since this pulseheight corresponds directly to the incoming X-ray photon energy, the measured energy also decreases. In addition, the spectral resolution degrades due to noise in the charge trapping and re-emission process, non-uniform trap distribution, and variations in trap occupancy. All of these processes apply to the charge in each pixel, so multi-pixel X-ray events will be more degraded than single-pixel events.

Measured CTI is a function of fluence, or, more specifically, the amount of charge deposited on the CCD. As the fluence increases, traps filled by one charge packet may remain filled as a second charge packet is transferred through the pixel. The second charge packet sees fewer unoccupied traps as a result of the previous "sacrificial charge" and loses less charge than it would have otherwise (Gendreau et al. 1993). This sacrificial charge can be in the form of X-rays, charged particle interactions, or intentionally injected charge.

The response of a CCD-based instrument is thus partially determined by its particle environment, whether causing radiation damage or providing sacrificial charge, which in turn is dependent on the spacecraft orbit. The Advanced CCD Imaging Spectrometer (ACIS) on the *Chandra X-ray Observatory* (Weisskopf et al. 2002) and the X-ray Imaging Spectrometer (XIS) on the *Suzaku X-ray Observatory* (Mitsuda et al. 2007) utilize similar CCDs but occupy very different radiation environments. The two instruments combined have produced more than twenty-two years worth of monitoring data which provide a unique opportunity to better understand the relationship between X-ray CCD spectral resolution, radiation damage, and the on-orbit particle background.

We begin by describing the differences and similarities of the instruments, spacecraft orbits, and on-board calibration sources in Section 2. Section 3 outlines our data analysis procedures while Section 4 discusses the results. The data used in this paper have been minimally processed and have not undergone standard pipeline processing which applies corrections to provide the best performance possible. The results here do not reflect what a typical user would find using standard data products.

2. Description of the Instruments

2.1. CCD Detector Characteristics

The CCD chips in ACIS and XIS were fabricated at MIT Lincoln Laboratory and are very similar in design. The ACIS CCDs predate the XIS CCDs by nearly a decade so some differences do exist.

Chandra has a single X-ray telescope and a moveable Science Instrument Module (SIM), which can move ACIS in and out of the telescope focus. The ACIS focal plane consists of ten CCD devices (MIT Lincoln Laboratory CCID17), eight of which are front-illuminated (FI) and two of which are back-illuminated (BI). The layout of the ACIS devices is shown in Figure 1. The CCD characteristics are summarized in Table 1 and described in detail by Garmire et al. (2003).

Suzaku has four XIS instruments, each with an independent X-ray Telescope (XRT) and focal plane assembly. The four devices are model CCID41, comprising three FI chips (XIS0, XIS2, and XIS3) and one BI (XIS1). The layout of the XIS devices is shown in Figure 2. One of the FI devices (XIS2) was damaged by a likely micrometeorite strike in October 2006 and has been unused since that time. The characteristics of the CCDs are summarized in Table 1 and described in detail by Koyama et al. (2007). The XIS devices are physically very similar to the ACIS devices with one notable exception, the addition of charge injection capabilities in the XIS CCID41 (Bautz et al. 2007). This allows a controlled amount of charge to be injected from a register at the top of the array into individual pixels, rows, or a variety of patterns as the CCD is clocked. The injected charge is transferred along with the other charge packets in the array.

While the CCDs are reasonably similar, there are a number of important operational differences. The individual frame exposure time for XIS is more than twice as long as for ACIS. Given the same particle or X-ray flux, the longer frame time of XIS will yield more sacrificial charge than seen on ACIS. Another important difference is the operating temperature of the detector. ACIS is kept much colder than XIS (−120°C versus −90°C), which reduces the incidence of warm pixels. Depending on the characteristics of the electron traps, the temperature can also change the measured CTI. In the case of the ACIS BI CCDs, the initial CTI is all due to the manufacturing process, and the initial performance is slightly better at warmer temperatures (Burke et al. 1997). The CTI of the ACIS FI CCDs is entirely due to radiation damage, so the CCDs are highly sensitive to temperature and have much lower CTI at −120°C (Grant et al. 2006). Similarly, the row-to-row transfer times are slightly different between ACIS and XIS, which, depending on the time constants of the electron traps, can change the measured CTI.

Finally, charge injection, while initially turned off for the XIS detectors, has been the standard operating mode since November 2006 (Uchiyama et al. 2009). In this mode a full row of charge is injected every 54 rows, or every 8.2 ms during the chip read out. Initially the level of injected charge was equivalent to 6 keV for the FI chips and was much lower, 2 keV, for the BI chip. The level of injected charge for the BI chip was increased to 6 keV in June 2011 (Tsujimoto et al. 2011; LaMarr et al. 2012).

As already noted above, between the time that ACIS and XIS were built, some improvements were made in the BI manufacturing process. The ACIS BI CCDs had measurable CTI across the entire array, including the frame store and serial readout array, from defects induced during the manufacturing process. The performance of the XIS BI CCD was nearly the same as the FI CCDs pre-launch, due to an improved thinning process further described in Burke et al. (2004) and Bautz et al. (2004).

For the purposes of this paper, we are only examining parallel CTI, or charge loss as a function of row number. Serial CTI, charge loss as a function of columns, is negligible for both XIS and ACIS except in the case of the ACIS BI CCDs, and even then it is not evolving on orbit (Grant et al. 2005).

2.2. Orbital Radiation Environments

ACIS and XIS occupy quite different radiation environments. *Chandra* is in a highly elliptical, 2.7-day orbit that transits a wide range of particle environments, from the Earth's radiation belts at closest approach through the magnetosphere and magnetopause and past the bow shock into the solar wind (O'Dell et al. 2000). Soon after launch it was discovered that the FI CCDs had suffered radiation damage from exposure to soft protons (∼0.1–0.5 MeV) scattered off *Chandra's* grazing-incidence optics during passages through the radiation belts (Prigozhin et al. 2000). The BI CCDs were unaffected due to the much deeper buried channel. Since the discovery of the radiation damage, ACIS has been protected during radiation belt passages by moving it out of the focal plane. Radiation damage to the CCDs has continued at a much slower rate, due to soft protons scattered by the optics during observations, and strongly penetrating solar protons and cosmic rays which pass through the spacecraft shielding. The particle background on the detector consists of a quiescent portion that is anti-correlated with the solar cycle, and soft proton flares (Grant et al. 2002).

Suzaku is in a 96-minute, low-Earth orbit with an inclination of 32 degrees and gains some protection from cosmic rays by the Earth's geomagnetic field (Mitsuda et al. 2007). Many orbits pass through the South Atlantic Anomaly (SAA), a region of enhanced particle flux, which requires the instruments to be shut off. The particle background on the XIS detectors is produced by cosmic rays that penetrate the spacecraft shielding (Mizuno et al. 2004); it is generally lower for XIS than for ACIS and varies throughout the orbit as a function of the geomagnetic cut-off rigidity, a measure of how well the Earth's geomagnetic field shields the spacecraft from charged particles (Tawa et al. 2008).

2.3. Calibration Sources

Both ACIS and XIS have on-board radioactive ^{55}Fe sources used for instrument monitoring and calibration. The ACIS External Calibration Source (ECS) is mounted such that it is only viewable when ACIS is moved out of the focal plane. Observations of the ECS are done twice an orbit, just before and after perigee passages. The ECS provides roughly uniform illumination of the entire focal plane. Fluorescent Al and Ti targets provide lines at 1.5 keV (Al K) and 4.5 keV (Ti Kα), as well as those from the ^{55}Fe source itself at ∼0.7 keV (Mn L), 5.9 keV (Mn Kα), and 6.4 keV (Mn Kβ).

The calibration sources on XIS illuminate the upper corners of each CCD during all observations. The spectral lines are from the ^{55}Fe source itself at 5.9 keV (Mn Kα), and 6.4 keV (Mn Kβ). The window of the source holder absorbs the low-energy Mn L lines. The orientation and approximate size of the regions illuminated by the calibration sources are shown in Figure 2.

The energy spectra of the ACIS and XIS calibration sources are shown in Figure 3. These data are from the BI CCDs taken early in each mission when performance was best. In the region around the Mn Kα line the spectra from the two sources look very similar to each other.

3. Methodology

3.1. Data and Analysis

The data used here have not gone through the standard pipeline processing that is normally applied to data distributed to users. Standard processing[1] is designed to remove some of the effects we are trying to study here, by applying corrections for CTI and

---

[1] See http://cxc.harvard.edu/ciao/threads/data.html and http://heasarc.gsfc.nasa.gov/docs/suzaku/analysis/abc/

time-dependent gain changes. The actual performance seen by a typical user from standard pipeline processed data is much improved from that reported here. These data have been minimally processed, by removing the CCD bias level and by applying a standard grade filter (ASCA G02346) and discarding all others event grades. XIS1 and ACIS-S3 are used are representative BI CCDs and XIS3 and ACIS-I3 are representative FI CCDs.

As the XIS calibration sources only illuminate the upper corners of the CCDs, we filter the data to include only events within a rectangular region encompassing the calibration source events. The size of the region varies slightly between CCDs, but is roughly 225 pixels square. While the ACIS calibration sources fully illuminate the CCDs, the ACIS data were also filtered to roughly match the XIS regions.

The individual calibration source observations are then grouped together by time in bins of roughly a month. The ACIS data cover the time period from January 2000, when the focal plane temperature was initially lowered to its current value, to May 2013. The XIS data begin shortly after the *Suzaku* launch in July 2005 and also continue through May 2013. The XIS data with and without charge injection and the XIS1 data with different levels of charge injection are binned separately, as the performance is quite different.

The gain of the detector, or the transformation from pulseheight to energy for each event, is determined by fitting a Gaussian to the pulseheight histogram in the initial time bin. The two corner regions must be fit separately, since they are in different readout nodes and do not have the same gain. This gain correction is then applied to all the time bins.

We then make an energy spectrum of the data in each time bin. Since we have already applied a gain correction, the two corner regions can be combined into one spectrum and fit together for better counting statistics. A Gaussian plus a linear background term is fit to the region around the Mn Kα line using Gehrels weighting (Gehrels 1986) which is a better approximation of the statistical error when the counts in the spectral bins can be small or zero. The Gaussian centroid and width are used in the subsequent sections of this paper to understand the evolution of CTI. Example spectra of the region around the Mn Kα line for the XIS FI CCD with and without charge injection are shown in Figure 4. Also shown are the best fit Gaussian plus background model.

3.2. A Proxy for Measuring CTI

A standard measurement of parallel CTI, or charge loss as a function of row, requires full illumination of the CCD with a source of known energy. The ECS on ACIS is capable of illuminating the entire CCD array with photons at a number of specific energies, as described in Section 2.3. The CTI on XIS is calibrated in a number of less direct ways, including a novel method of “checker flag” charge injection described further in Ozawa et al. (2009). Since the XIS calibration sources are incapable of illuminating the full chip, for proper comparison we must restrict our analysis to the upper corners of the ACIS chips as well. A change in CTI must change the accumulated charge loss and thus the pulseheight far from the frame store region. A change in pulseheight, however, does not necessarily have to be related to CTI in the imaging array; it could also be due to CTI changes in the frame store or changes in the gain completely unrelated to radiation damage. For example, ACIS has a known slow change in the gain as a function of time as measured very close to the frame store where imaging array CTI change should be negligible. For most of the CCDs it is monotonically decreasing at a rate of ~ 2.4 eV or 0.04% per year at 5.9 keV.[2]

To determine the feasibility of using only the upper corners as a CTI metric, we compared the change in Mn Kα pulseheight to the measured CTI for two ACIS chips. The results are shown in Figure 5. Prior to correcting for the known gain change, the fractional pulseheight change is well-correlated to the CTI (left panels). After the correction, the correlation is even tighter (right panels). The correction coefficient was fit by eye, finding the value that best reduced the ACIS-I3 scatter. The correction is always less than 0.5% of the total pulseheight.

While the electronics of the two instruments are not identical, there’s no reason to assume this should change the dependence of the line centroid on CTI. It is possible, however, that the harder spectrum of the particle radiation in low Earth orbit compared to *Chandra’s* higher orbit could produce changes in the CTI of the XIS frame store array. To further test this, we have examined multiple XIS observations of the Perseus cluster which is large enough to illuminate a substantial area of the CCDs and has been observed numerous times. The cluster spectrum has a strong line due to He-like iron at 6.5 keV (observed frame), which can be used, like the Mn Kα line in the calibration source, to directly measure the change in line energy as a function of row. We can then extrapolate this relation to find the line energy at row zero as a function of time. This value should be insensitive to increased radiation damage in the imaging array, and only dependent on changes in the frame store or changes in the electronic gain.

Figure 6 shows this line energy change as a function of time. All the data shown were taken with charge injection active, but before the BI charge injection level was increased. The change in line energy independent of the imaging array CTI is 0.6% per year for XIS1 and 0.2% per year for XIS3. The difference between XIS1 and XIS3 may indicate that the cause for the line energy change is radiation damage in the frame store, rather than an electronics gain change. Radiation damage in the frame store is partially mitigated by the charge injection, and since the amount of injected charge is smaller for the BI CCD, it receives less mitigation. The amount of injected charge is smaller for the BI CCD than it is for the FI CCD, so it receives less mitigation. If so, these can be considered lower limits for the line energy change in the frame store when charge injection is not active and cannot mitigate the charge loss due to radiation damage. After the XIS1 charge injection level was increased, we assume that the line energy change in the frame store of XIS1 should be equal to that on XIS3.

4. Discussion

4.1. CTI Time Evolution

We measure the time evolution of CTI using the change in line energy of the Mn Kα line, as described in the previous section. The change in line energy is plotted in Figure 7 (for XIS) and Figure 8 (for ACIS) as the fractional change since the first data point. Data from both front- and back-illuminated devices are included, as well as both with and without XIS charge injection.

Increasing CTI leads to decreasing measured line energy. All cases show an overall increase in CTI due to radiation damage. In some cases, the CTI increase from radiation damage is modified by sacrificial charge from the particle background, discussed

---

[2] See http://space.mit.edu/home/cgrant/gain for example plots of the gain change.

further in Section 4.3. Charge injection also clearly modifies the rate of CTI increase. The rate of change of CTI varies substantially between the different cases.

4.1.1. Suzaku

The use of charge injection for the XIS greatly affects the inferred change in CTI. Charge injection was not used from the beginning of the *Suzaku* mission through mid-2006; the rate of line energy change is roughly 2.0% per year for the BI device and 1.9% per year for the FI device during this time (see Figure 7). The FI and BI devices, while not identical, appear very similar and the line energy evolution is approximately linear with time. We can remove the affects of frame store CTI by assuming that the FI and BI line energy evolution would be about the same with the same level of charge injection. As we showed in Section 3.2, the change in the BI is larger than that in the FI, presumably because the BI uses a lower level of injected charge. We can use the BI value (0.6% per year) as a lower limit for the case of no charge injection for both the BI and FI. Then in the absence of charge injection, the upper limit of the line energy change in just the imaging array is about 1.4% per year for the BI device and 1.3% per year for the FI device.

When charge injection was first turned on in 2006, there were three notable changes. The first is that the line energy is restored to nearly its original value, since the charge injection produces significant sacrificial charge which improves the measured CTI. The second is that the rate of change of line energy is shallower with charge injection than without. Finally, the improvement due to charge injection is larger for the FI CCD than for the BI device. The rate of line energy change is roughly 1.0% per year for the BI CCD and 0.36% per year for the FI CCD. After removing the gain change measured in Section 3.2, the rate of line energy change is roughly 0.40% per year for the BI CCD and 0.16% per year for the FI CCD.

The FI/BI difference in 2006 is due to the fact that the amount of charge injected is higher for the FI CCD than for the BI CCD (Bautz et al. 2007). In particular, for the FI CCD the injected charge level, 6 keV, is higher than the X-ray line energy of the calibration source and for the BI CCD the charge level, 2 keV, is much lower than the line energy. The amount of charge injection on the BI CCD is insufficient to provide the full potential mitigation. The amount of injected charge on the BI CCD was increased in mid-2011 to be equal to the FI CCD and since that time the rate of line energy change of the BI CCD is 0.34% per year, nearly the same as the FI CCD (LaMarr et al. 2012). After removing the gain change measured in Section 3.2, the rate of line energy change for the BI CCD with 6 keV charge injection is roughly 0.14% per year.

4.1.2. Chandra

The change in line energy for ACIS is very different from XIS, as can be seen in Figure 8. ACIS does not have the capability to inject a known quantity of charge like XIS, so the only sacrificial charge is from the particle background and the X-ray photons themselves. The rate of line energy change is much lower for ACIS than it is for XIS and is also more irregular, particularly for the FI CCD. Assuming a linear decrease, the change is roughly 0.12% per year for the BI CCD and 0.10% per year for the FI CCD. After removing the known gain change discussed in Section 3.2, the change in ACIS line energy is roughly 0.08% per year for the BI CCD and 0.06% for the FI CCD.

The evolution of the FI and BI CCDs look quite different from each other as well. The FI CCDs are much more sensitive to sacrificial charge from the particle background than the BI CCDs. The FI CCD decrease is clearly not strictly linear, due to the changing sacrificial charge which adds both features from individual solar storms and a larger modification tied to the solar cycle. This is seen in distinct features common to the plots of line energy and particle backgrounds as a function of time; periods of low background correspond to periods of increased CTI, and vice versa (see Figure 9). This FI/BI distinction cannot be due to differences in the number and type of particles impinging on the CCDs because they are in the same orbital environment, but must result from how the particles interact with the CCD structure. Sacrificial charge from the changing particle background and the FI/BI difference will be discussed further in Section 4.3.

4.2. Spectral Resolution Time Evolution

The spectral resolution is measured as the FWHM of the Mn Kα line. The time evolution of spectral resolution is shown in Figures 10 and 11 for XIS and ACIS, respectively. Data from both front- and back-illuminated devices are included, as well as both with and without XIS charge injection.

The relationship between increasing CTI and spectral resolution is not as simple as that for line energy. If an X-ray event occupies a single pixel, the charge loss due to CTI essentially adds an additional noise term to the spectral resolution, which would increase in step with the increased charge loss. In the case of both ACIS and XIS, many events are split over multiple pixels. In that case, charge loss adds additional noise terms from all of the split pixels. In addition, some of the lost charge may be re-emitted into a trailing pixel which may or may not also be included in the event pulseheight depending on the size of the trailing charge and the original split charge. The combined effects of these processes result in a broader FWHM than would be measured in the absence of CTI.

4.2.1. Suzaku

The spectral resolution of the XIS devices shows temporal effects from both CTI and operational changes (see Figure 10). Initially, before charge injection was turned on, the rate of increase of spectral resolution for FI and BI CCDs was very similar, about 50 eV per year. Once charge injection was turned on, the performance improved and FWHM dropped to nearly the initial value. The rate of increase is much slower with charge injection than without, although again, the FI CCD shows more improvement than the BI CCD due to the larger amount of injected charge in the FI devices. The FWHM increase is about 9 eV per year for the FI CCD and about 13 eV per year for the BI CCD. As discussed in Section 4.1.1, after the increase in the amount of injected charge on the BI CCD in mid-2011, the rate of FWHM change for the BI CCD improves to about 7 eV per year, very similar to the FI CCD.

4.2.2. Chandra

The spectral resolution time dependence for ACIS differs from that of XIS (see Figure 11). The initial FWHM for both ACIS devices is much higher than that for XIS. This is due to the prelaunch manufacturing defects on the BI CCD (see Section 2.1) and the initial radiation damage to the FI CCDs in 1999 (see Section 2.2). The rate of increase, however, is vanishingly small, less than 1 eV per year for the BI CCD and consistent with no change for the FI CCD. Unlike the line energy, the FWHM evolution shows no obvious dependence on the particle background.

4.3. CTI and Spectral Resolution: Dependence on Background

As stated previously, measured CTI is a function of the amount of charge deposited on the CCD. Increasing the amount of sacrificial charge improves performance and lowers CTI. Figure 12 shows images of typical raw CCD frames for both ACIS and XIS and both types of CCDs. Essentially all the visible features are due to cosmic ray charged particles. While the images do include X-ray events from the calibration sources and (in the case of XIS) celestial sources, they are nearly invisible due to their small size and low numbers. In the absence of controlled charge injection, as is now routine on *Suzaku*, the most important source of sacrificial charge is from particle interactions.

The most obvious distinction is that between the FI and BI CCDs due to their structural differences. The FI CCDs display large streaks and blobs while the BI CCDs have much smaller features. The FI CCDs have an active, depleted region and a much thicker field-free region in the silicon substrate. The X-ray events generally interact in the depleted region so the charge is collected in a small area. Charged particles can traverse the entire thickness of the CCD, depositing charge along their path. The charge in the field-free region can disperse more freely and produces the large blobs seen in the image. The BI CCDs are fully depleted, without the additional field-free region. The charge from particles stays more concentrated into smaller blobs and streaks. Comparing the FI and BI images from a single instrument, such as ACIS, shows that the total number of particle hits is comparable even though their morphology is so different.

The number of particle events is different between XIS and ACIS. ACIS clearly shows more particle events than XIS, even though the ACIS frame exposure time, 3.2 sec, is less than half that of XIS, 8 sec. This is due to the particle environment in the two orbits. *Suzaku* is in a low-earth orbit and receives substantial shielding from the Earth's magnetic field while *Chandra's* orbit takes it well above the magnetosphere and does not receive the same shielding.

This can also be seen in Figure 13 which shows the particle background spectrum from each instrument after event recognition and filtering. The ACIS data was taken while the instrument was stowed and not under its calibration source, while the XIS data was taken looking at the dark Earth. In both cases, the only X-rays are due to materials fluorescing in the instrument with the remainder of the events from particle interactions. Both XIS CCDs have much lower particle background levels than ACIS, due to the different orbits. The BI devices have higher levels than the FI devices, as the larger cosmic ray blooms seen on the FI CCDs are more efficiently filtered out of the event list. All the devices have the same pixel size, so the comparison is valid.

One might assume that the higher particle rate on the ACIS raw frames would translate to faster accumulation of radiation damage, but that is not necessarily the case. One reason is that the raw frames and the particle spectra represent only a snapshot of the relative particle rates at a particular time. Both orbits intersect regions with much higher particle rates (Earth's radiation belts and the SAA) that will not be seen in the data as the instruments are shut down. The total radiation dosage needs to consider the environment during the entire orbit and during times of high solar activity, not just while data are being collected. A second reason is that the measured CTI (Figures 7 and 8) is a function not only of the accumulated radiation damage, but also the sacrificial charge and the focal plane temperatures (see Section 4.4).

These basic distinctions in the number and morphology of particle events can explain some of the differences between the CTI evolution of ACIS and XIS. An additional piece of the puzzle is the time-dependence of the particle events themselves. Figure 9 shows a measure of the ACIS particle background over the same time period and with the same binning as the line energy evolution data. In this case the rate of high energy events rejected on-board the spacecraft is used as a proxy for the particle rate. These events are well above the X-ray energies that can be focused by the telescope and can only be caused by particles. The particle background rate is clearly not constant but is lowest in 2001, reaches more than twice that level in 2010, and is nearly back to the original low level in 2013. It has been shown that this measure of the ACIS particle background is well correlated over long time-scales with proton fluxes measured by the Advanced Composition Explorer (Stone et al. 1998) spacecraft with energies above 10 MeV (Grant et al. 2002). The lower particle fluxes are due to extra shielding provided by the solar magnetic field during solar maximum. Additional smaller scale dips can be seen which can be directly linked to increased heliomagnetic shielding during specific solar storms. The solar storms also produce transient increases in the particle background, but these are over much shorter timescales, hours to days, and thus do not appear in Figure 9.

We can use these dips in the line energy to quantify the strength of its dependence on sacrificial charge from the particle background. A correction for sacrificial charge is part of the ACIS instrument team's standard CTI monitoring program described in Grant et al. (2005), although the correction factors have evolved since then. We can apply these correction factors to our line energy data to get a better sense for the true CTI change in the absence of sacrificial charge from the particle background. This corrected line energy and the line energy with no correction are shown in Figure 14. The CTI evolution is now much smoother, with a slightly higher rate of increase during solar maximum (2000–2002). After removing the gain change discussed in Section 3.2 and assuming a linear dependence, the rate of change is now 0.08% and 0.17% per year for the BI and FI CCDs, respectively, as compared to the background-uncorrected values of 0.08% and 0.06% per year. The FI device is clearly much more sensitive to sacrificial charge than the BI device.

Due to the shielding from the Earth's magnetic field, the long-term variability of the XIS particle background is very small. Tawa et al. (2008) found that after removing the orbital modulation and with the exception of a brief period of high solar activity, the particle background on XIS was constant within ±6% per year. We have verified that the broad-band (5–13 keV) particle background in all three XIS detectors has changed by less than 4% per year for the range of dates considered in this work.

A much stronger variability is induced by the Earth's geomagnetic field as the spacecraft travels about its ~96-minute orbit. Geomagnetic cut-off rigidity (COR) quantifies the shielding provided by the geomagnetic field at a particular orbital position. High values of COR correspond to regions with higher shielding and therefore lower particle background. In particular, we are using the quantity COR2, as defined in Tawa et al. (2008). The count rate of the particle background more than doubles between the highest and lowest COR values (Tawa et al. 2008).

The dependence of line energy on cut-off rigidity is shown in Figure 15. In general, line energy is only weakly dependent on cut-off rigidity, and that dependence disappears when charge injection is active. In the absence of charge injection, the line energy varies by about 0.2% over the entire range of COR values for both the BI and FI CCDs, with slightly higher line energies at low COR, as is expected for sacrificial charge from the particle background. With charge injection, this minimal dependence disappears, as the injected charge completes overwhelms the charge from the particle background.

The ACIS FI CCD line energy appears to have a much stronger dependence on sacrificial charge from the particle background than the ACIS BI CCD or XIS. Over the entire range of ACIS particle background rates, about a factor of two, the line energy change due to sacrificial charge is about 1.5% for the FI CCD and about 0.01% for the BI CCD. Without charge injection, the XIS line energy changes by only about 0.2% for both BI and FI CCDs over the entire range of COR values, which is also about a factor of two in particle rates. As discussed before, the absolute level of the particle background is much higher for ACIS than for XIS. For example, in the typical raw images shown in Figure 12, the total charge per frame from both particles and X-rays is more than two times higher for ACIS than for XIS. While this does make sacrificial charge more important for ACIS than XIS, the two ACIS CCD types are seeing the same particle flux and yet have different sacrificial charge dependencies.

The sacrificial charge differences between the BI and FI CCDs on ACIS are partially due to the structural differences; the spatial distribution of the deposited charge is much more compact on the BI than on the FI CCD. More important is that both types of ACIS CCDs start the time period covered here with significantly more CTI than XIS and the source of the CTI for each is distinct. The FI CCDs were damaged very early in the mission from unprotected passages through the Earth's radiation belts, while the BI CCD initial CTI is entirely due to manufacturing. The types of electron traps that are causing the charge loss are not the same and the typical de-trapping timescales will also be different. Grant et al. (2005) demonstrates this by comparing the fraction of the lost charge that is re-emitted into the following pixel. It is an order of magnitude higher for the BI CCD than the FI, implying the the BI CCD traps have much shorter time constants. The time constants of the FI CCD traps are better matched to the typical frequency of sacrificial charge due to cosmic rays and thus their performance is much more sensitive to the cosmic ray rate (Grant et al. 2003). The XIS sacrificial charge dependence is identical between the FI and BI CCDs since both the original CTI and the accumulated CTI are similar. Presumably the time constants of the XIS traps are shorter than the typical frequency of cosmic ray sacrificial charge.

In contrast to the line energy evolution, the line width for ACIS does not appear to have any dependence on the changing sacrificial charge. None of the strong features seen in the line energy and particle background (Figure 9) are seen in Figure 11. This does not imply that the presence or absence of sacrificial charge has no effect on the spectral resolution, just not on the timescales dealt with in this work. Grant et al. (2003) developed an event-level pulseheight correction for the FI CCD that used additional information on the distance and amount of sacrificial charge along the readout path which did provide some improvement of the line width. Because the time constants of the FI CCD traps are well matched to the typical frequency of cosmic ray sacrificial charge, the random distribution of the cosmic rays produces additional noise in the spectral resolution. The overall level of cosmic rays, as mapped in this work, does not appear to be as important. The ACIS BI CCDs, as discussed above, have trap time constants that are shorter, so both the pulseheight and the line width are reasonably independent of the sacrificial charge.

The XIS line width, however, does show a weak dependence on cut-off-rigidity in the absence of charge injection and varies by about 15 eV over the entire range of COR values (Figure 16). As it was for the XIS line energy, this dependence disappears with the use of charge injection, which overwhelms the charge from the particle background.

4.4. CTI and Spectral Resolution: Dependence on Temperature

At least some of the differences between the evolution of CTI on ACIS and XIS can possibly be due to operating at different focal plane temperatures. ACIS is kept much colder at −120°C than XIS at −90°C, so many of the common electron traps that cause CTI have been frozen out. To best measure the differences in performance, we want to minimize the effect of the sacrificial charge, both from the particle background on ACIS and charge injection on *Suzaku*. We can compare the line energy evolution of ACIS after the sacrificial charge correction discussed in the previous section (Figure 14) to XIS without charge injection (Figure 7). The rate of change is much higher for XIS than for ACIS by a factor of about 18 for the BI CCDs and 7 for the FI CCDs. While this could be due to a higher level of damaging particle radiation, it could also be due to the higher CCD temperatures.

Fortunately, the ACIS team has performed a series of CTI measurements at different temperatures on two occasions separated by six years (Grant et al. 2006). We can use these data to compare the time evolution at −120°C and −90°C, determine how large the CTI change on ACIS would be at either temperature, and then compare to the actual change measured for XIS to see how much of the difference is due to temperature rather than anything else. We have reanalyzed the data used in Grant et al. (2006) to duplicate the data analysis techniques used in this paper. The representative FI CCD in this paper, ACIS-I3, was not in use during the first set of temperature measurements, so it is replaced in the analysis of this paragraph by ACIS-S2 which should have similar characteristics. We can only compare the line energy and not the line width evolution, as the much higher level of CTI on ACIS makes measurement of the width at warm temperatures problematic. The change in line energy with time is approximately a factor of four times larger at −90°C than at −120°C. This can be compared to the much larger ratio between the ACIS and XIS line energy change in the previous paragraph. Scaling the ACIS line energy evolution to −90°C yields a rate of change of 0.3%/yr (BI) and 0.5%/yr (FI), which is still much smaller than the XIS rate of change. While temperature can explain some of the difference between the line energy evolution of ACIS and XIS, it cannot account for all of the difference.

5. Conclusions

We have compared the on-orbit performance evolution of the *Chandra* ACIS and *Suzaku* XIS CCDs, which share similar hardware, to better understand the effect of the radiation environment in low- and high-Earth orbit. Both instruments have suffered performance degradation due to radiation damage, but operational differences make this comparison more complicated. Most important are the presence of charge injection and the warmer focal plane temperature on XIS.

The change in line energy with time was used as a proxy for measuring changing charge transfer inefficiency. To reduce confusion with changes in the electronic gain and CTI in the frame store array, we have removed our best estimates of this change. The XIS CCDs show strong, linear time evolution with very weak dependence on the particle background. Applying charge injection slows the rate of CTI increase and removes the particle background dependence entirely. Both BI and FI devices have similar rates of change. The ACIS CCDs exhibit much slower time evolution than XIS, with strong particle background dependence in the FI devices and much weaker dependence in the BI devices. The ACIS FI and BI devices do not have similar rates of change, with the FI devices showing stronger evolution than the BI devices.

The most equivalent comparison is XIS without charge injection to ACIS after removing the sacrificial charge from the particle background. The rate of line energy decrease is 1.4%/yr (BI) and 1.3%/yr (FI) for XIS with no charge injection, and 0.08%/yr (BI) and 0.18%/yr (FI) for ACIS after removing the improvement due to sacrificial charge. To compensate for the different focal plane temperatures, we can use the results of Grant et al. (2006) described in Section 4.4 to scale the ACIS data taken at $-120°$C, to our best estimate of what it would be at $-90°$C, the focal plane temperature for the XIS devices. This increases the ACIS rate of change to 0.3%/yr (BI) and 0.5%/yr (FI), which is still much smaller than the rate of change seen by XIS.

Even after compensating for the differences due to temperature and due to sacrificial charge from the particle background and charge injection, the rate of line energy decrease and CTI increase is much higher for XIS than for ACIS, which implies that the radiation dosage received by the CCDs in low Earth orbit is larger than that seen in high orbit. This is the reverse of what one might assume based on Figure 13, which shows that the particle background spectrum as seen by the XIS CCDs is lower than that on ACIS, however as explained in Section 4.3, this is only a snapshot of the relative particle rates at a particular time and ignores the potentially much higher rates during times when the instruments are not taking data (Earth's radiation belts and the SAA).

In addition, the FI and BI devices on XIS have essentially the same line energy evolution, while on ACIS, the FI devices change much faster than the BI. This tells us something about the energy distribution of the damaging particles; that at least some of the damage to the ACIS CCDs is from softer particles with insufficient energy to reach the deeper buried channel in the BI CCDs (i.e. ~0.1–0.5 MeV protons), while the damage to the XIS CCDs must be primarily from higher energy particles. The initial radiation damage to ACIS from unprotected passages through the radiation belts was entirely to the FI CCDs, not the BIs. While the radiation dosage was large, the particles were all soft protons. The continuing damage is to both types of ACIS CCDs, although the rate of change on the FI CCDs is three times that of the BIs, so the damaging particles must be a mix of hard and soft energies. The XIS CCDs, on the other hand, have nearly identical continuing damage.

The dependence of spectral resolution evolution on radiation damage is more complicated than it is for line energy. The stochastic nature of charge loss adds width to the spectral resolution, but this is further complicated by multi-pixel events and the interplay of charge loss and trailing. The combination of these processes broadens the FWHM. Neither ACIS nor XIS show strong dependence of FWHM on sacrificial charge. Without charge injection, the XIS line width increases by about 50 eV/yr, which charge injection reduces to just under 10 eV/yr. ACIS, on the other hand, shows little to no increase in the spectral resolution, however the line width was much higher than XIS to begin with and may be so large as to swamp the smaller incremental changes.

This comparison of XIS and ACIS performance evolution emphasizes the importance of the orbital environment. The low-Earth orbit of *Suzaku* has the advantage of a much lower and stable particle background during observations than *Chandra* which is of great value particularly in studies of extended faint objections. The *Chandra* particle background during observations is much higher and subject to variations due to the solar cycle and solar storms. This is in contrast to the accumulated radiation damage which is higher for *Suzaku* even after correcting for differences in operating temperature and sacrificial charge. The addition of charge injection for the *Suzaku* XIS CCDs provides substantial performance improvement. While the choice of orbit for future missions is obviously dependent on many factors beyond the radiation environment, we hope this study will be useful for better informing that choice.

Acknowledgements. The authors thank blah blah and blah blah for such and such. This work was supported by NASA contracts NAS 8-37716, NAS 8-38252, and NNX-09AE58G, and by funding from the Institute of Space and Astronautical Science, Japan Aerospace Exploration Agency. **need to double-check funding stuff with Mark.**

References

Bautz, M. W., Kissel, S. E., Prigozhin, G. Y., et al. 2004, in Society of Photo-Optical Instrumentation Engineers (SPIE) Conference Series, Vol. 5501, Society of Photo-Optical Instrumentation Engineers (SPIE) Conference Series, ed. A. D. Holland, 111–122

Bautz, M. W., LaMarr, B. J., Miller, E. D., et al. 2007, in Society of Photo-Optical Instrumentation Engineers (SPIE) Conference Series, Vol. 6686, Society of Photo-Optical Instrumentation Engineers (SPIE) Conference Series

Burke, B. E., Gregory, J. A., Bautz, M. W., et al. 1997, IEEE Transactions on Electron Devices, 44, 1633

Burke, B. E., Gregory, J. A., Loomis, A. H., et al. 2004, IEEE Transactions on Nuclear Science, 51, 2322

Garmire, G. P., Bautz, M. W., Ford, P. G., Nousek, J. A., & Ricker, Jr., G. R. 2003, in Society of Photo-Optical Instrumentation Engineers (SPIE) Conference Series, Vol. 4851, Society of Photo-Optical Instrumentation Engineers (SPIE) Conference Series, ed. J. E. Truemper & H. D. Tananbaum, 28–44

Gehrels, N. 1986, ApJ, 303, 336

Gendreau, K., Bautz, M., & Ricker, G. 1993, Nuclear Instruments and Methods in Physics Research A, 335, 318

Grant, C. E., Bautz, M. W., Kissel, S. E., LaMarr, B., & Prigozhin, G. Y. 2006, in Society of Photo-Optical Instrumentation Engineers (SPIE) Conference Series, Vol. 6276, Society of Photo-Optical Instrumentation Engineers (SPIE) Conference Series

Grant, C. E., Bautz, M. W., Kissel, S. M., LaMarr, B., & Prigozhin, G. Y. 2005, in Society of Photo-Optical Instrumentation Engineers (SPIE) Conference Series, Vol. 5898, Society of Photo-Optical Instrumentation Engineers (SPIE) Conference Series, ed. O. H. W. Siegmund, 201–211

Grant, C. E., Bautz, M. W., & Virani, S. N. 2002, in Astronomical Society of the Pacific Conference Series, Vol. 262, The High Energy Universe at Sharp Focus: Chandra Science, ed. E. M. Schlegel & S. D. Vrtilek, 401

Grant, C. E., Prigozhin, G. Y., LaMarr, B., & Bautz, M. W. 2003, in Society of Photo-Optical Instrumentation Engineers (SPIE) Conference Series, Vol. 4851, Society of Photo-Optical Instrumentation Engineers (SPIE) Conference Series, ed. J. E. Truemper & H. D. Tananbaum, 140–148

Koyama, K., Tsunemi, H., Dotani, T., et al. 2007, PASJ, 59, 23

LaMarr, B. J., Bautz, M. W., Kissel, S. E., Miller, E. D., & Prigozhin, G. Y. 2012, in Society of Photo-Optical Instrumentation Engineers (SPIE) Conference Series, Vol. 8443, Society of Photo-Optical Instrumentation Engineers (SPIE) Conference Series

Mitsuda, K., Bautz, M., Inoue, H., et al. 2007, PASJ, 59, 1

Mizuno, T., Kamae, T., Godfrey, G., et al. 2004, ApJ, 614, 1113

O'Dell, S. L., Bautz, M. W., Blackwell, W. C., et al. 2000, in Society of Photo-Optical Instrumentation Engineers (SPIE) Conference Series, Vol. 4140, Society of Photo-Optical Instrumentation Engineers (SPIE) Conference Series, ed. K. A. Flanagan & O. H. Siegmund, 99–110

Ozawa, M., Uchiyama, H., Matsumoto, H., et al. 2009, PASJ, 61, 1
Prigozhin, G. Y., Kissel, S. E., Bautz, M. W., et al. 2000, in Society of Photo-Optical Instrumentation Engineers (SPIE) Conference Series, Vol. 4140, Society of Photo-Optical Instrumentation Engineers (SPIE) Conference Series, ed. K. A. Flanagan & O. H. Siegmund, 123–134
Stone, E. C., Frandsen, A. M., Mewaldt, R. A., et al. 1998, Space Sci. Rev., 86, 1
Tawa, N., Hayashida, K., Nagai, M., et al. 2008, PASJ, 60, 11
Tsujimoto, M., Miller, E. D., Murakami, H., et al. 2011, in JX-ISAS-SUZAKU-MEMO-2010-07 (ftp://legacy.gsfc.nasa.gov/suzaku/doc/xis/suzakumemo-2010-07v4.pdf)
Uchiyama, H., Ozawa, M., Matsumoto, H., et al. 2009, PASJ, 61, 9
Weisskopf, M. C., Brinkman, B., Canizares, C., et al. 2002, PASP, 114, 1

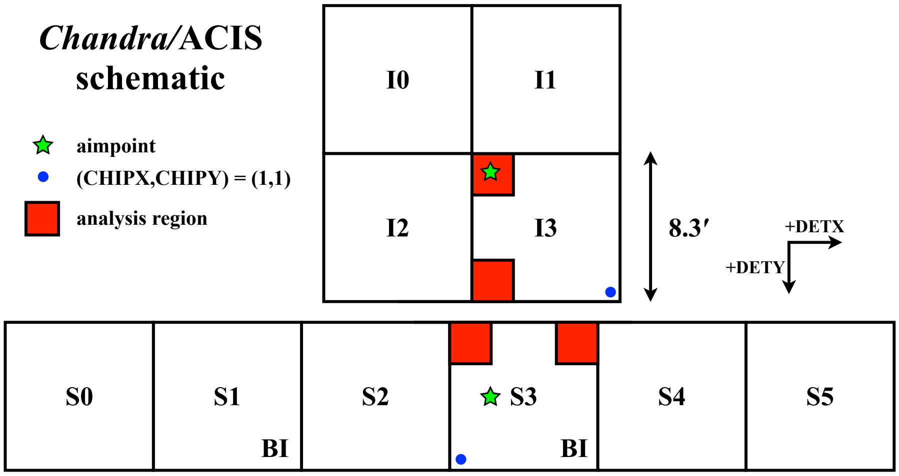

Fig. 1. Schematic drawing of the ACIS focal plane. The red squares indicate the regions used for data analysis in this paper. The green stars show the standard aimpoints on ACIS-I3 and ACIS-S3.

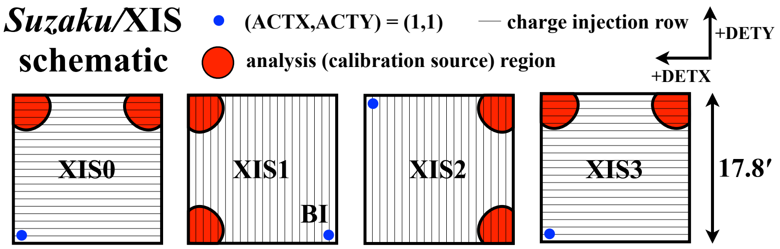

Fig. 2. Schematic drawing of the XIS focal plane. The red circles show the regions illuminated by the ^{55}Fe sources. The light grey lines indicate the direction and spacing of the charge injection rows.

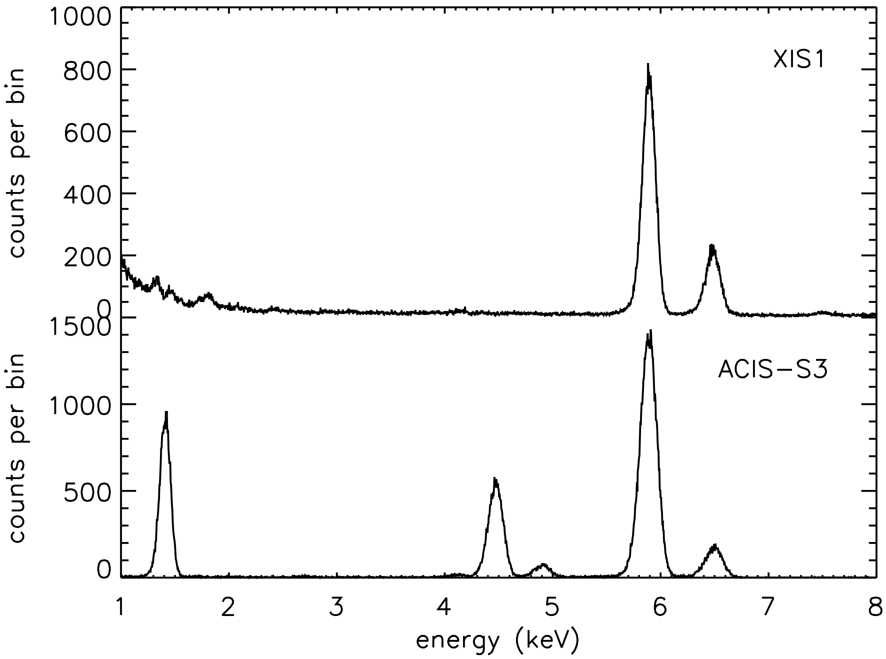

Fig. 3. Example spectra of the XIS and ACIS calibration sources using the BI CCDs taken early in each of the missions when performance was best. Both sources have strong Mn Kα and Mn Kβ lines around 6 keV. The ACIS source has additional lines from titanium and aluminum.

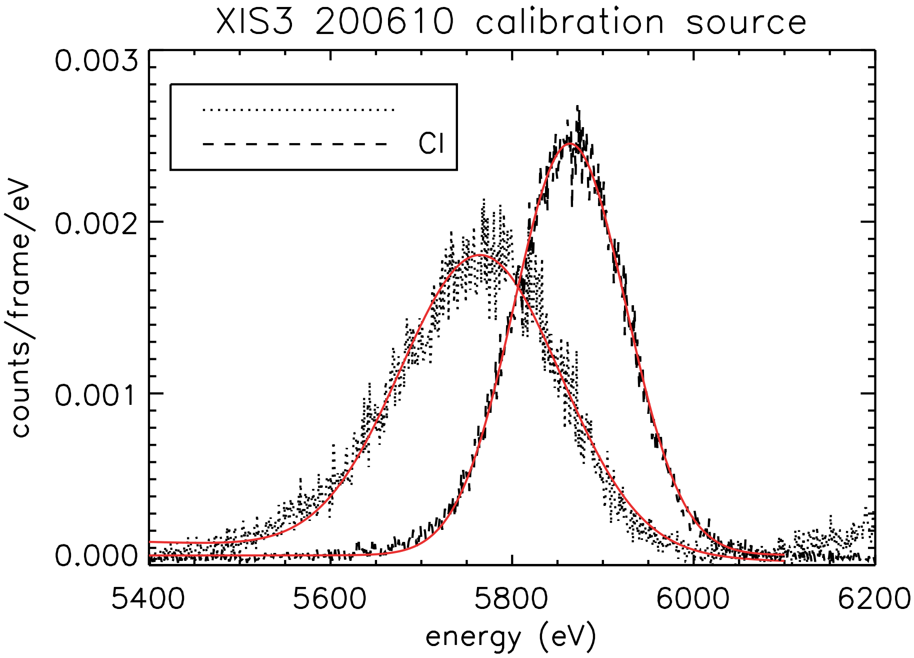

Fig. 4. Spectrum of the Mn Kα line at 5.9 keV for the XIS FI CCD. Without charge injection (dotted line), the line is broader and shifted to lower energies. Charge injection (dashed line) improves both the line centroid and the width. The red line is the best fit Gaussian plus linear background.

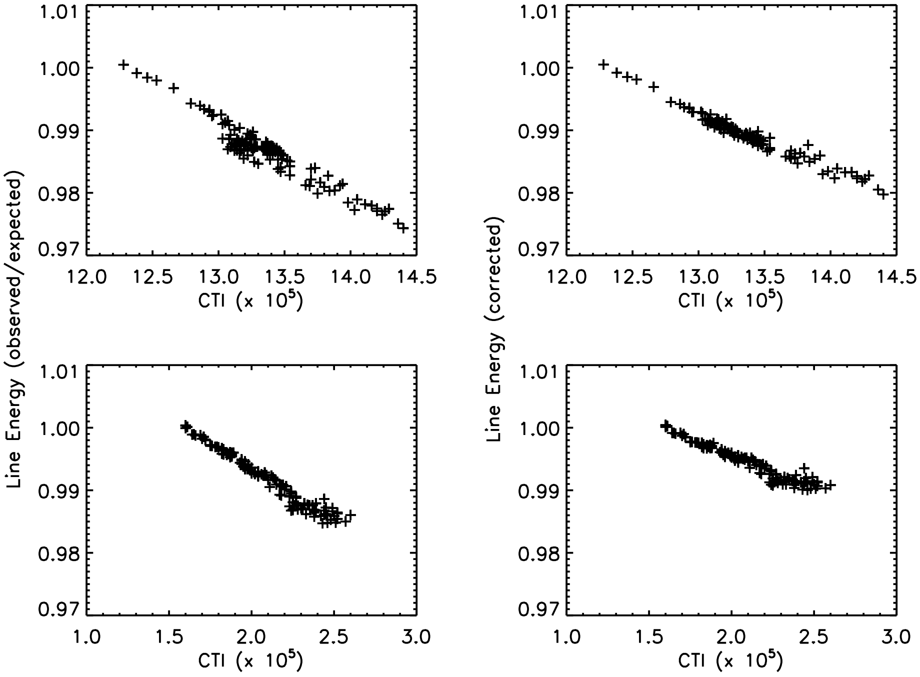

Fig. 5. Charge Transfer Inefficiency ($\times 10^5$) versus the fractional change in Mn Kα line energy for two ACIS devices, the FI CCD I3 (top) and the BI CCD S3 (bottom), as measured from the upper corners of each chip. The left panels show the measured data, while the right panels show data corrected for a slow gain decrease, discussed in the text. The CTI and pulseheight are well-correlated.

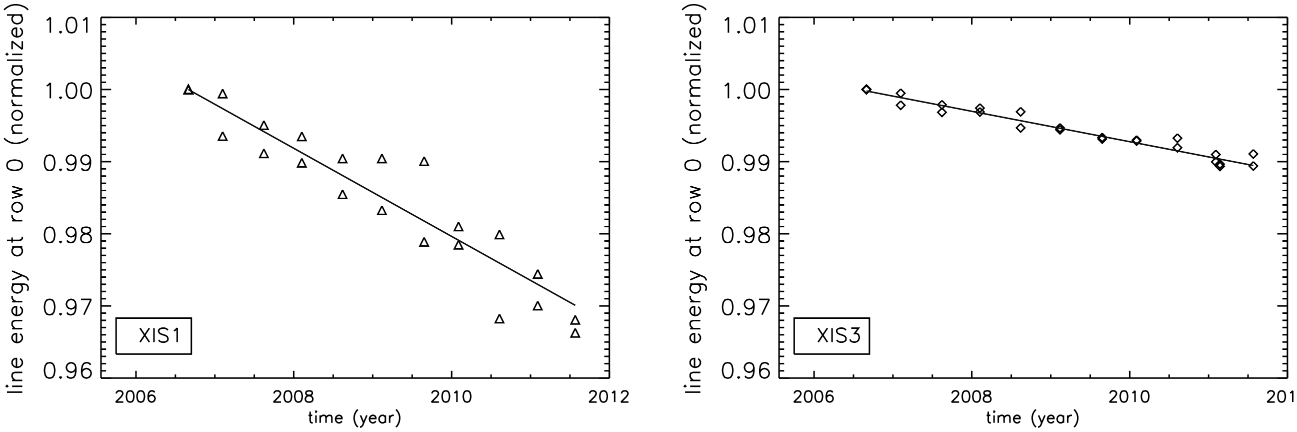

Fig. 6. Fractional change in the XIS line energy at the bottom of the imaging array, measured using the iron line in observations of the Perseus cluster. Each observations has two data points, one from each of the two central quadrants of the CCD. All the data shown were taken with charge injection active, but before the XIS1 charge injection level was increased to match XIS3.

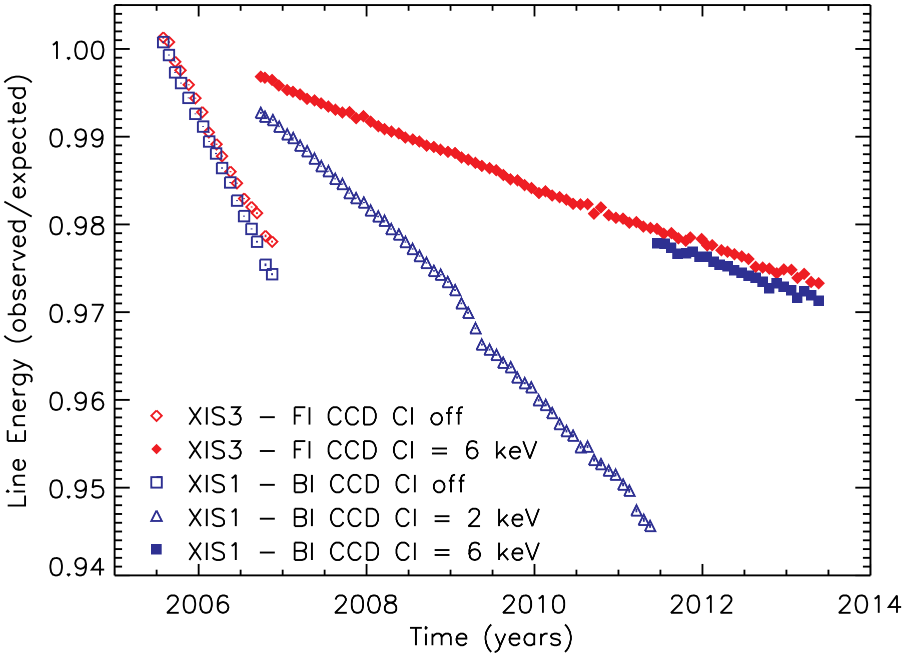

Fig. 7. Fractional change in the XIS line energy over the course of the *Suzaku* mission, as measured at Mn Kα. Different symbols show FI and BI devices with charge injection (CI) on and off. The BI device utilized a lower level of injected charge, 2 keV, until mid-2011 when CI was raised to match the FI device. The 1-σ error bars are shown but are much smaller than the symbol sizes.

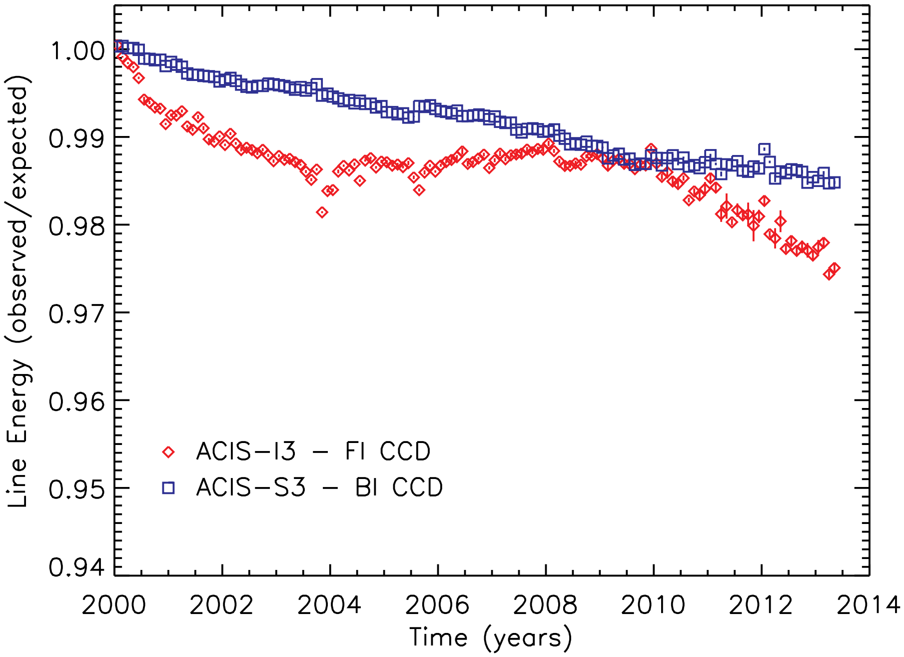

Fig. 8. Fractional change in ACIS line energy over the course of the *Chandra* mission, as measured at Mn Kα. The effects of varying particle background and sacrificial charge are seen in the ACIS-I3 (FI) data. The 1-σ error bars are shown but are often smaller than the symbol sizes.

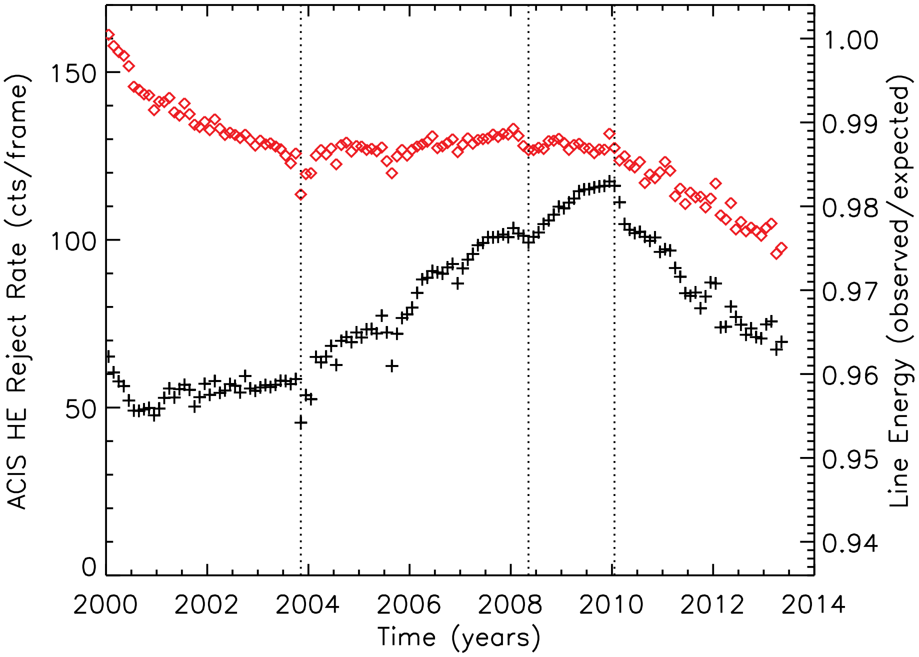

Fig. 9. Time history of the particle background of the *Chandra* mission, measured as the rate of high energy events on ACIS-S3 (BI), shown as black crosses. The time period and binning are the same as the CTI evolution data. The structure from the varying particle background can been seen in the ACIS FI CCD line energy data, shown in red. The vertical lines demonstrate the simultaneous nature of the structures.

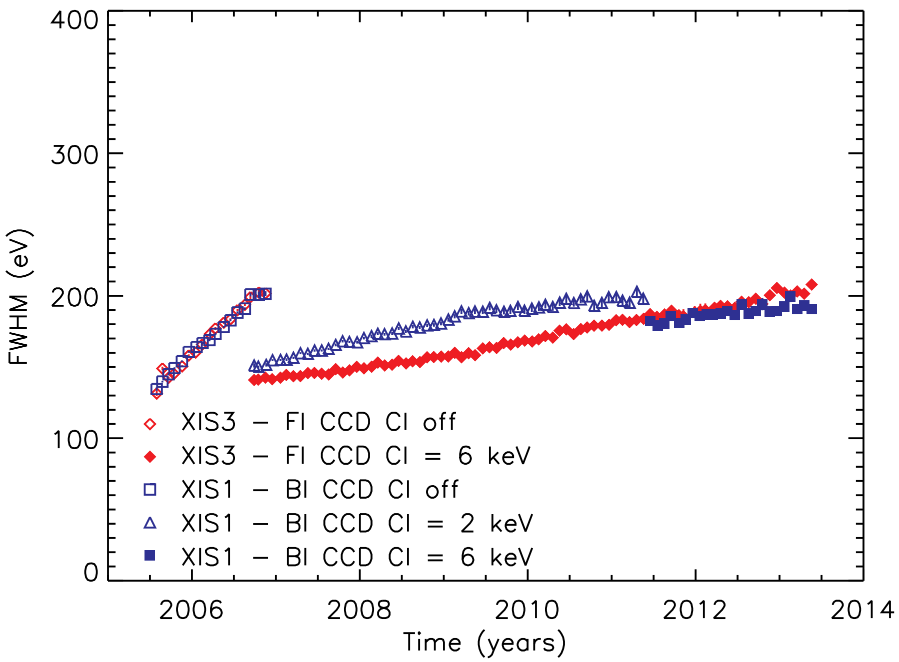

Fig. 10. Change in XIS line width (FWHM) with time over the course of the *Suzaku* mission, as measured at Mn Kα. Different symbols show FI and BI devices with charge injection (CI) on and off. The 1-σ error bars are shown but are often smaller than the symbol sizes.

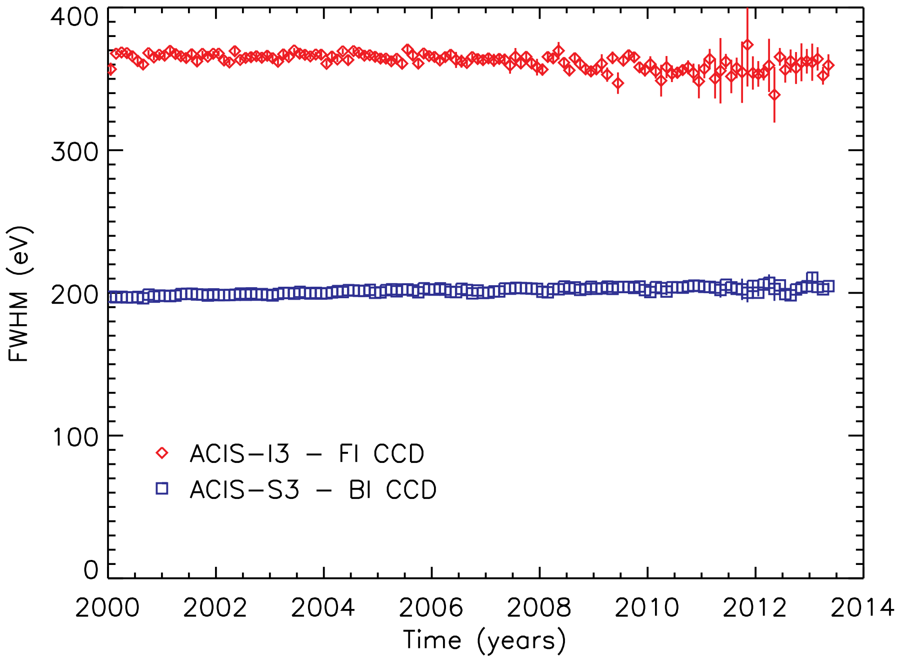

Fig. 11. Change in ACIS line width over the course of the *Chandra* mission, as measured at Mn Kα. The 1-σ error bars are shown but are often smaller than the symbol sizes.

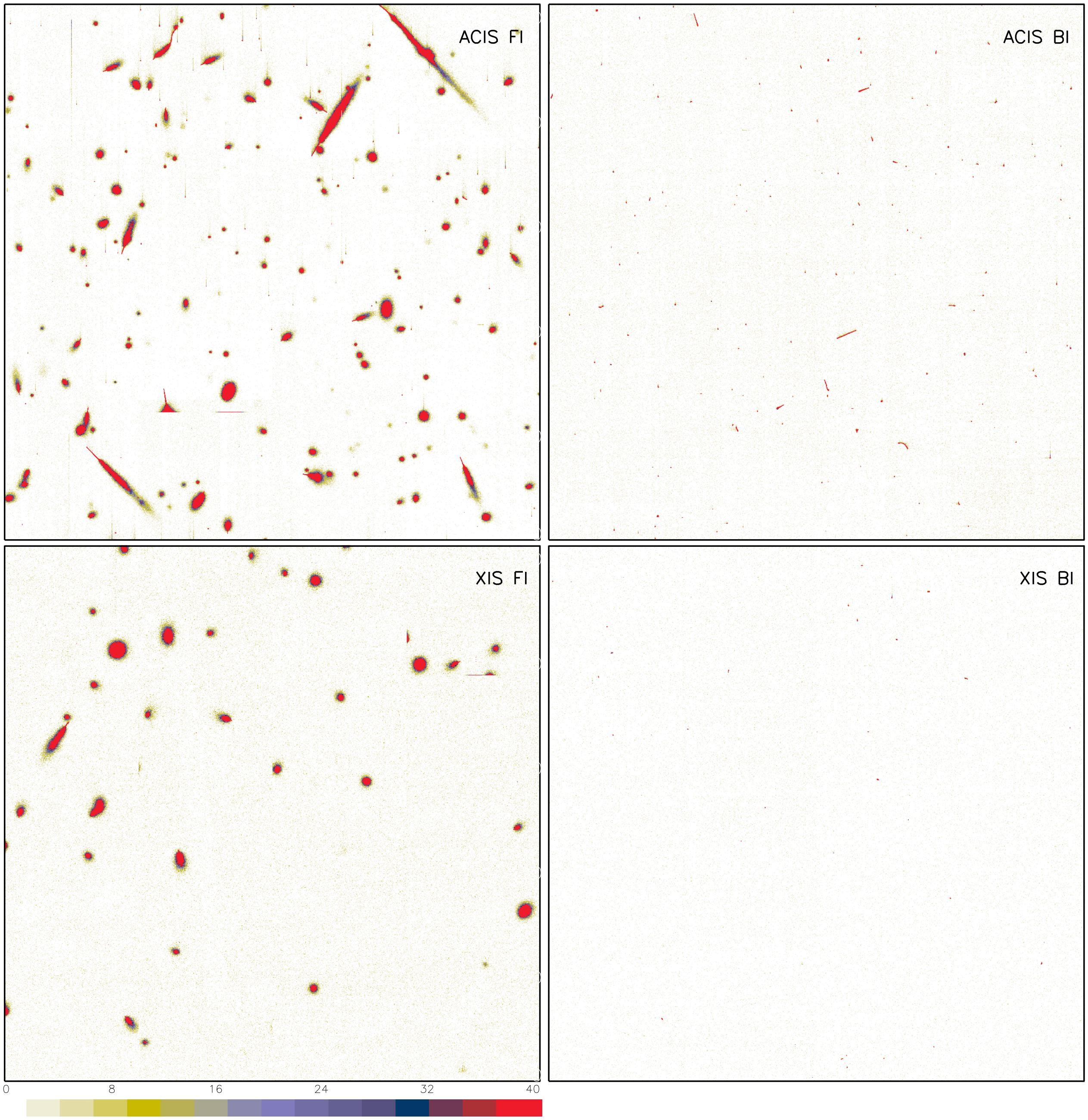

Fig. 12. Typical raw frame images for ACIS (top) and XIS (bottom), showing an FI (left) and BI (right) device for each. The color bar shows the pixel values in ADU. An X-ray event from ^{55}Fe would have a pulseheight around 1500 ADU. Each image is 1024 by 1024 pixels. The differences between the FI and BI CCDs, and between ACIS and XIS are explained in the text.

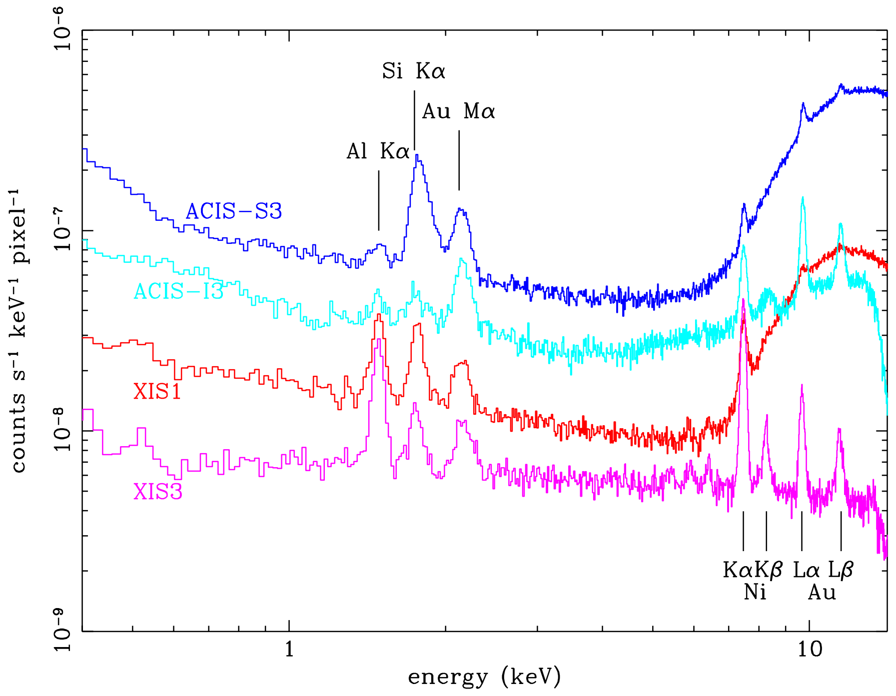

Fig. 13. Spectrum of the particle background seen by ACIS and XIS after standard event detection and filtering. The rate of particle events is higher for ACIS compared to XIS due to the different orbits. The BI CCDs have a higher rate of particle events than the FI CCDs, due to their structural differences. The larger blooms produced by particles on the FI CCD are more efficiently filtered in the event selection process than on the BI CCD.

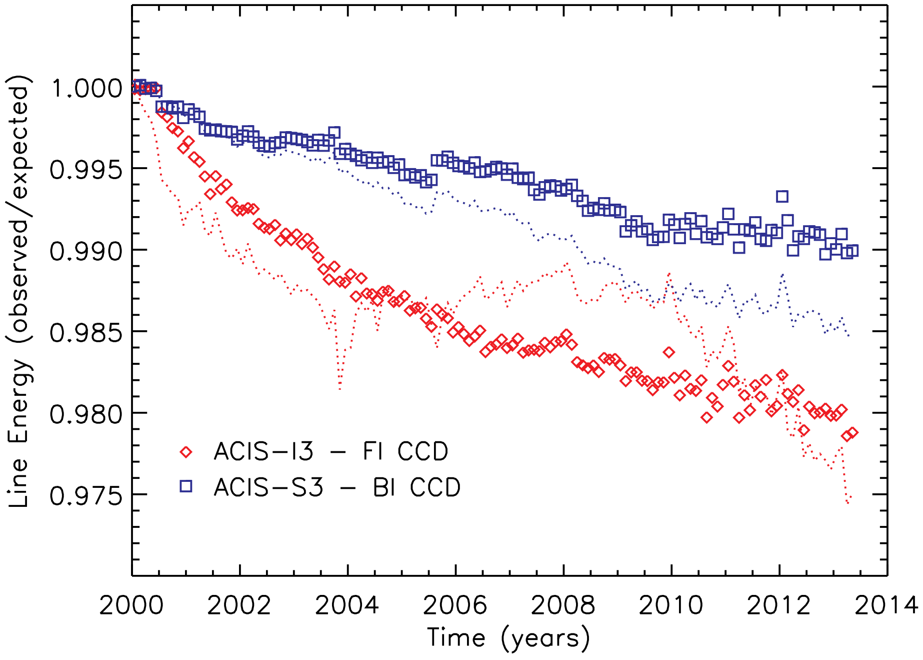

Fig. 14. Fractional change in ACIS line central energy over the course of the *Chandra* mission, after correcting for sacrificial charge from the particle background. For comparison, the dotted lines show the uncorrected line energy as in Figure 8.

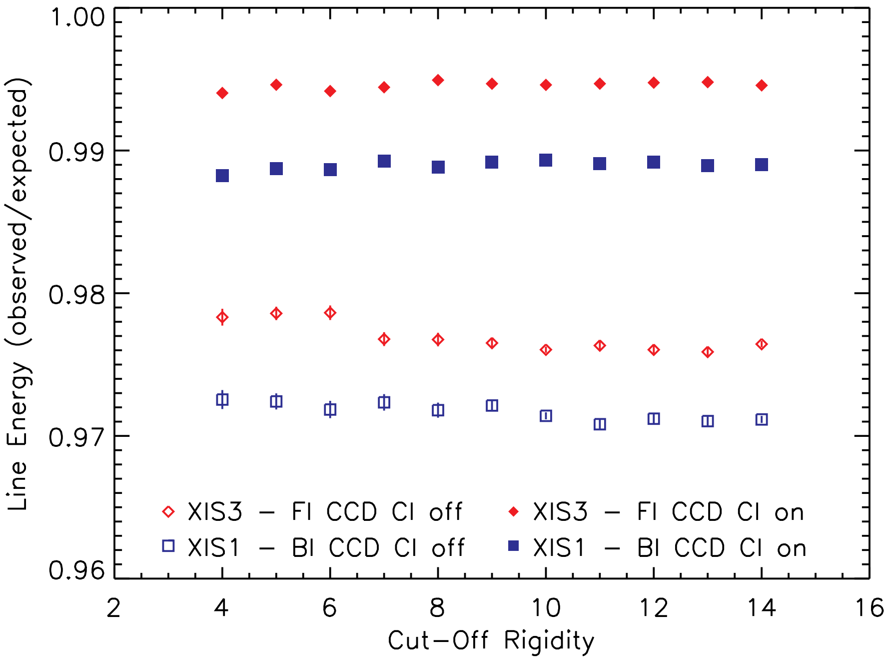

Fig. 15. Fractional change in the XIS line energy as a function of geomagnetic cut-off rigidity (COR), averaging over October-November 2006. Symbols are the same as in Figure 7. Without charge injection, there is a weak dependence of line energy with COR, with higher line energy associated with lower COR, as is expected for sacrificial charge. The use of charge injection overwhelms the effects of sacrificial charge from the particle background (solid symbols). The 1-σ error bars are shown but are often smaller than the symbol sizes.

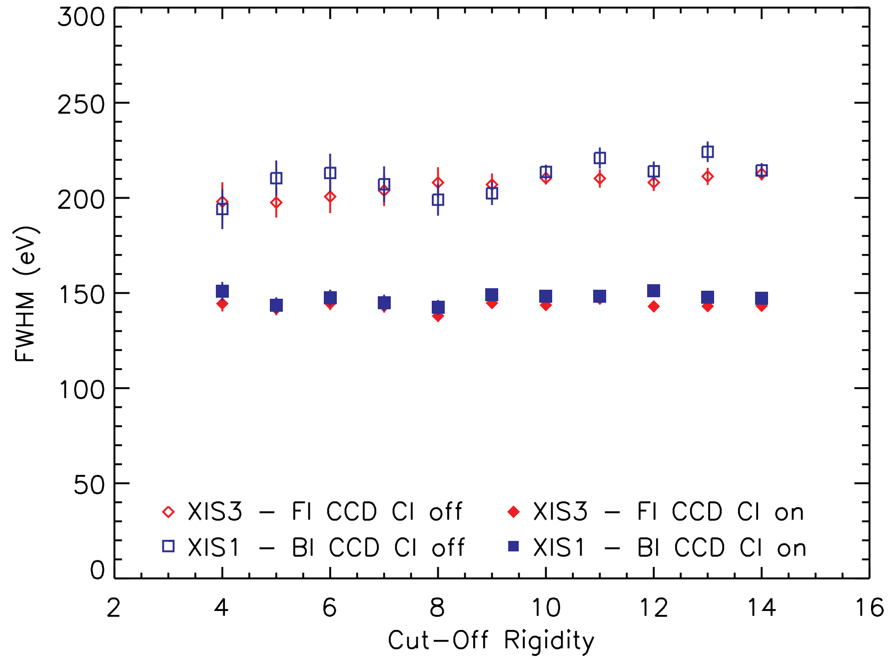

Fig. 16. XIS Mn Kα line width (FWHM) as a function of COR, averaging over October-November 2006. Symbols are the same as in Figure 10. Lower cut-off rigidity indicates a higher particle background, therefore the narrower line widths at low COR in the absence of charge injection (open symbols) are due to sacrificial charge. Use of charge injection overwhelms the effects of sacrificial charge, so no dependence on COR is seen in those data (solid symbols).

Table 1. Characteristics of MIT Lincoln Laboratory CCDs for ACIS and XIS

	ACIS	XIS
Model	CCID17	CCID41
Format	1026 rows × 1024 pixels/row (imaging area)	
Architecture	3-phase, frame-transfer, four parallel output nodes	
Illumination Geometry	8 FI & 2 BI	2 FI & 1 BI
Charge Injection Capable	no	yes
Pixel Size	$24 \times 24\ \mu$m	
Readout Noise (RMS)	2–3 e^- at 400 kpix s^{-1}	< 2.5 e^- at 41 kpix s^{-1}
Depletion Depth	FI: 64–76 μm; BI: 30–40 μm	FI: 60–65 μm; BI: 40–45 μm
Operating Temperature	−120°C via radiative cooling	−90°C via Peltier cooler
Frame Transfer Time (per row)	40 μs	24 μs (CI off); 152 μs (CI on)
Frame Exposure Time[a]	3.2 s	8.0 s
Pre-Launch CTI (10^{-5})	FI: < 0.3	FI: 0.3–0.5
	BI: 1–3	BI: 0.55

(a) In normal operating mode.